

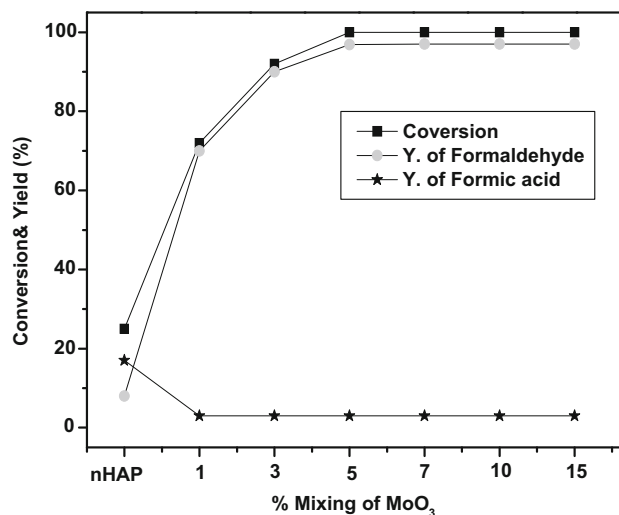
# Selective Oxidation of Methanol to Formaldehyde Over Active Molybdenum Oxide Supported on Hydroxyapatite Catalysts

Abd El-Aziz A. Said<sup>1</sup> · Mohamed M. M. Abd El-Wahab<sup>1</sup> · Alian M. Alian<sup>1</sup>

Received: 26 July 2015 / Accepted: 2 September 2015  
© Springer Science+Business Media New York 2015

**Abstract** Hydroxyapatite (HAP) was synthesized by sol-gel method. Different ratios of molybdenum oxide (1–15 % w/w) supported on HAP were prepared by the impregnation method and calcined at 400 °C in a static air atmosphere. The catalysts were characterized by thermogravimetry, differential thermal analysis, X-ray diffraction, FTIR spectroscopy and nitrogen sorption measurements. The surface acidity of the catalysts was investigated by the dehydration of isopropyl alcohol and the adsorption of pyridine (PY) and 2,6-dimethyl pyridine (DMPY). The gas-phase oxidation of methanol to formaldehyde was carried out in a conventional fixed-bed flow type reactor using N<sub>2</sub> as a carrier gas. The obtained results clearly revealed that HAP–MoO<sub>3</sub> systems were active and selective towards the formation of formaldehyde. The maximum yield of formaldehyde (97 %) was achieved on the catalyst containing 5 wt% MoO<sub>3</sub>/HAP. The generation of Mo<sup>6+</sup> as Lewis together with Brønsted acid sites play the main role in the formation of formaldehyde.

**Graphical Abstract** Catalytic oxidation of methanol over MoO<sub>3</sub>/HAP calcined at 400 °C for 4 h.



**Keywords** MoO<sub>3</sub> · Hydroxyapatite · Surface area · Acidity · Oxidation · Methanol

## 1 Introduction

Methanol, one of the most important chemical intermediates, used in chemical industry. It is the starting material for the synthesis of various products such as hydrocarbons and oxidation products [1]. Formaldehyde production is the major one among the oxidation processes. Two processes are generally used in the industry to produce formaldehyde, both using methanol as the starting material [2]. The dehydrogenation of methanol-rich air mixture over silver catalyst and direct oxidation of methanol-poor air mixture over iron molybdate catalyst. Both processes are still in use [3]. The choice between silver and iron molybdate catalysts

✉ Abd El-Aziz A. Said  
aasaid55@yahoo.com

<sup>1</sup> Chemistry Department, Faculty of Science, Assiut University, Assiut, Egypt

must be based not only on economic aspect, but should also take into account the product end-use, size of plant and the type of operation [4].

Methanol oxidation into formaldehyde occurs selectively on MoO<sub>3</sub> loaded on such weak basic supports as SnO<sub>2</sub>, Fe<sub>2</sub>O<sub>3</sub> and ZrO<sub>2</sub>, among which SnO<sub>2</sub> has the most prominent effect [5]. The effect of the support on the activity is an interesting chemical aspect to understand the role of support on the metal oxide. A lot of investigations on the prominent effect of the support have been reported in the literature [6–8]. It was concluded that acidity was a key parameter to control the activity for methanol oxidation [9]. On the other hand hydroxyapatite (HAP) has attracted the attention of researchers to the biomaterials field in recent years [10]. HAP is a highly non-stoichiometric calcium phosphate compound with a Ca/P molar ratio ranging from 1.5 to 1.67. It is also known [11] to have the character of both acidic and a basic character. Moreover, HAP as support offers high stability and various substitutions are allowed by the apatite structure [12]. Various transition metal cations, which have potential as catalytic active centers, can be readily accommodated into the apatite framework based on the large cation exchange ability of HAP [13–15]. In addition sol–gel synthesis of HAP has attracted much attention [16–19]. This method offers a molecular-level mixing of the calcium and phosphorus precursors, which is capable of improving the chemical homogeneity of the resulting HAP to a significant extent, in comparison with conventional methods such as solid state reactions [20], wet precipitation [21] and hydrothermal synthesis [22].

However, the catalytic gas phase oxidation of methanol over MoO<sub>3</sub> supported on nano hydroxyapatite synthesized by sol–gel method to our best knowledge has not been reported except our recent short work [23]. Therefore, the objective of the present study was devoted to the study of MoO<sub>3</sub> supported on hydroxyapatite in detail as an efficient and competitive catalyst for conversion of methanol to formaldehyde.

## 2 Experimental

### 2.1 Materials

Methyl alcohol, citric acid, calcium nitrate, diammonium hydrogen phosphate and ammonium hydroxide were obtained as pure reagents and were used without further purification. Ammonium heptamolybdate was supplied from Merck, (Darmstadt, Germany).

### 2.2 Synthesis of Hydroxyapatite by Sol–Gel Method

The citric acid sol–gel method [24] using Ca(NO<sub>3</sub>)<sub>2</sub>·4H<sub>2</sub>O, C<sub>6</sub>H<sub>8</sub>O<sub>7</sub>·4H<sub>2</sub>O and (NH<sub>4</sub>)<sub>2</sub>HPO<sub>4</sub> as starting materials,

ammonia solution as agent for pH adjustment. A suspension of 0.24 M Ca(NO<sub>3</sub>)<sub>2</sub>·4H<sub>2</sub>O in 350 mL bi-distilled water was vigorously stirred and its temperature was maintained at 75 °C. A solution of 0.29 M (NH<sub>4</sub>)<sub>2</sub>HPO<sub>4</sub> in 250 mL bi-distilled water was slowly added dropwise to Ca(NO<sub>3</sub>)<sub>2</sub>·4H<sub>2</sub>O and citric acid solution. In all experiments, the pH of the solutions was adjusted to 11. The hydroxyapatite (HAP) was filtered, washed with bi-distilled water, dried overnight at 100 °C and calcined in air at 400 °C for 4 h.

### 2.3 Preparation of MoO<sub>3</sub> Supported on Hydroxyapatite Catalysts

The catalysts were prepared by the impregnation method. Calculated amounts of (NH<sub>4</sub>)<sub>6</sub> Mo<sub>7</sub>O<sub>24</sub>·4H<sub>2</sub>O (AHM) (1–15 wt%) dissolved in bi-distilled water were admixed carefully with calculated amounts of hydroxyapatite. The samples produced were dried in an oven at 100 °C for 24 h before being calcined at 400 °C for 4 h in the static air atmosphere, and then quenched to room temperature.

### 2.4 Apparatus and Techniques

#### 2.4.1 Thermal Analysis

Thermogravimetry (TG) and differential thermal analysis (DTA) curves were recorded upon heating up to 700 °C at 10 °C min<sup>-1</sup> and a 40 ml min<sup>-1</sup> flow of air atmosphere, using a computerized Shimadzu Thermal Analyzer TA60 Apparatus (Japan).

#### 2.4.2 X-ray Diffraction

X-ray diffraction (XRD) analysis of the catalysts was performed with a Philips (The Netherlands) diffractometer (Model PW 2103,  $\lambda = 1.5418 \text{ \AA}$ , 35 kV and 20 mA) with a source of CuK $\alpha$  radiation (Ni filtered). An online data acquisition and handling system facilitated the automatic JCPDS library search and match for phase identification purposes. The crystallite size (*d*), of the synthesized catalysts was calculated using the following Debye–Scherrer formula [25],

$$(d) = K\lambda/B \cos \theta$$

The shape factor, *K*, was taken as 0.9, while  $\lambda$  for Cu K $\alpha$  radiation is 1.5418 Å. Where  $\lambda$  is the wavelength of the X-ray (nm), *B* is the full width of a diffraction peak under consideration (rad) in the middle of its height that was considered after computer-fit of the X-ray data using the Gaussian line, shape, and  $\theta$  is Bragg's angle, that is obtained using (1 1 1) line of the pure silicon as the standard.

### 2.4.3 FTIR Spectroscopy

FT-IR spectra of the prepared catalysts calcined at 400 °C for 4 h were recorded using a Nicolet spectrophotometer, model (6700), equipped with data station in the range of 2000–400 cm<sup>-1</sup> with a KBr disc technique.

### 2.4.4 Nitrogen Sorption

Nitrogen gas adsorption–desorption isotherms were measured at -196 °C using a Nova 3200 instrument (Quantachrom Instrument Corporation, USA). Test samples were thoroughly outgassed for 2 h at 200 °C to a residual pressure of 10<sup>-5</sup> torr, and the weight of the outgassed sample was that used in the calculation. The specific surface area, S<sub>BET</sub> was calculated by applying the Brunauer–Emmett–Teller (BET) equation. The porosity of the catalysts was determined from the desorption curves using Nova enhanced data reduction software (Version 2, 13).

### 2.4.5 Acidity Determination

The acidity of 10 wt% MoO<sub>3</sub>/HAP catalyst was determined by studying the dehydration of isopropyl alcohol (IPA), the adsorption of pyridine (PY) and 2,6-dimethyl pyridine (DMPY). The dehydration reaction of IPA was carried out in a conventional fixed bed flow Pyrex glass tube reactor, at atmospheric pressure using N<sub>2</sub> as a carrier gas. The reaction conditions were: 500 mg catalyst weight, 2 % reactant of IPA in the gas feed, 100 mL min<sup>-1</sup> total flow rate and 220 °C reaction temperature. The adsorption of PY and DMPY were carried out by injection of different volumes at steady state conditions, according to the previous method [26]. The effect of reaction temperature on the activity variation of presaturated catalyst towards IPA dehydration was tested. The strength of acid sites was investigated by DSC measurement. About 10 mg of pyridine-saturated sample was subjected to DSC analysis. The DSC analysis was recorded on heating from room temperature up to 400 °C with a heating rate of 10 °C min<sup>-1</sup> and 30 ml min<sup>-1</sup> flow of N<sub>2</sub>, using Auto Q20 DSC with mass flow apparatus (USA).

### 2.4.6 Catalytic Activity Measurements

The catalytic activity of the catalysts for the vapor-phase oxidation of methanol was carried out at 400 °C in a conventional fixed-bed flow type reactor at atmospheric pressure using dry nitrogen as a carrier gas. A 500 mg of catalyst was placed in the middle of the reactor with quartz wool. Space in the reactor pre-and post-heating zone was filled with glass beads to reduce the effect of auto-oxidation of the substrate and products in the gas phase. A

methyl alcohol and nitrogen were introduced into the reactor after nitrogen was bubbled through methyl alcohol saturator. The total flow rate was fixed at 100 mL min<sup>-1</sup> with 1.6 % reactant of methanol in the gas feed. The connection between the reactor and the gas chromatograph (GC) was heated by resistance wire to prevent any condensation. The reaction products were chromatographically analyzed by FID with a Unicam ProGC using a DNP glass column (2 m). Measurements of the conversion and yield (%) were recorded after 2 h from the initial introduction of methyl alcohol into the reactor to ensure the attainment of the reaction equilibrium, (steady state conditions). The degree of methanol conversion, selectivity and yield of formaldehyde are calculated as follows [27]:

$$\text{Conversion (\%)} = \frac{[\text{CH}_3\text{OH}]_{\text{in}} - [\text{CH}_3\text{OH}]_{\text{out}}}{[\text{CH}_3\text{OH}]_{\text{in}}} \times 100$$

$$\text{Selectivity (\%)} = \frac{[\text{Product}]}{[\text{CH}_3\text{OH}]_{\text{in}} - [\text{CH}_3\text{OH}]_{\text{out}}} \times 100$$

$$\text{Yield (\%)} = \frac{(\text{Conversion} \times \text{Selectivity})}{100}$$

In the previous equations, [CH<sub>3</sub>OH]<sub>in</sub> and [CH<sub>3</sub>OH]<sub>out</sub> denote the peak areas (concentrations) of methanol at the reactor inlet and outlet, respectively.

## 3 Results and Discussion

### 3.1 Thermal Analysis

Figure 1 shows the TG and DTA, curves of pure hydroxypatite (HAP), and ammonium heptamolybdate (AHM) supported on HAP. The TG and DTA curves of pure HAP exhibit four steps of weight loss that are accompanied with two endothermic peaks minimized at 130, 185 °C and two exothermic peaks maximized at, 264 and 445 °C. From these curves it is evident that, on heating the parent of HAP up to 200 °C, TG curve is displaying two weight losses. The first may correspond to the physically adsorbed water and the second belongs to the removal of the structure water molecules. On increasing the heating up to 700 °C, two losses steps with exothermic peaks maximized at 264 and 445 °C. These two steps may be attributed to the removal of ammonium nitrate from the gel and crystallization of Ca<sub>10</sub>(PO<sub>4</sub>)<sub>6</sub>(OH)<sub>2</sub> [24, 28–30] respectively.

TG and DTA curves of AHM supported on HAP reveal that the loss of weights are maximized at 130, 200 and 445 °C as indicated by the DTA curves. The first region of (30–150 °C) which accompanied with ~4.8 % weight loss with endothermic peak minimized at 130 °C is attributed to the removal of physically adsorbed water. The second step is in the range of (150–250 °C) which accompanied with ~43.4 % weight loss with exothermic peak maximized at

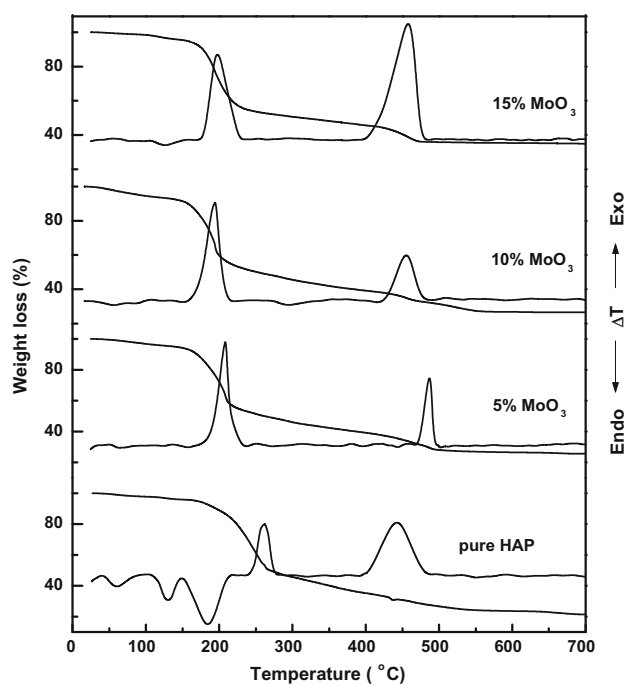


**Fig. 1** TG and DTA curves of pure HAP and AHM supported on HAP

200 °C due to the removal of structural water and/or decomposition of organic constituents [31]. The third region of (400–500 °C) which accompanied with ~16.8 % weight loss with exothermic peak maximized at 475 °C corresponds to the formation of  $\text{CaMoO}_4$  spinel. Moreover, no weight loss is observed on heating up to 700 °C. This means that  $\text{CaMoO}_4$  formed at lower temperatures is stable spinel [32, 33]. So, our findings were found much satisfied with the results that reported by Klinkaewnarong et al. [30] and Eslami et al. [33].

### 3.2 X-ray Diffraction Analysis

X-ray diffraction (XRD) patterns of the pure HAP, pure  $\text{MoO}_3$  and  $\text{MoO}_3$  supported on HAP calcined at 400 °C was carried out. Phase analysis was done using PDF card no. 85-0585 for  $\text{CaMoO}_4$ , which provide information on the  $2\theta$  range of 4°–80°. The patterns of the as-synthesized HAP powder calcined at 400 °C is presented in Fig. 2. It shows that there are several peaks i.e. (111), (002), (210), (211), (300), (202), (222), (213) and (004) are identical to those of the reference. It is clear from the figure that, the sample containing  $\text{MoO}_3$  with a ratio of (10 wt%) on HAP shows new peaks. These peaks may be attributed to the formation of a new phase nanocrystalline  $\text{CaMoO}_4$ . In addition, all of the prominent peaks corresponding to the  $\text{CaMoO}_4$  phase were appeared clearly without any peaks assigned to either, HAP, CaO and  $\text{CaCO}_3$ . These results are

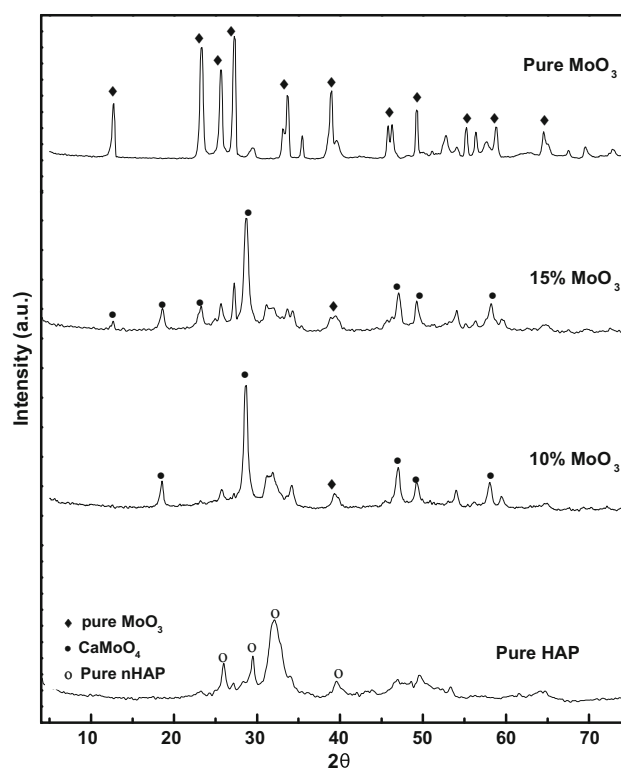


**Fig. 2** X-ray diffraction of pure HAP, pure  $\text{MoO}_3$  and  $\text{MoO}_3$  supported on HAP calcined at 400 °C for 4 h

in agreement with that were reported by Yoon et al. [32]. On the other hand, a small peak detected corresponding to  $\text{MoO}_3$ , start to appear with the addition of 15 wt%  $\text{MoO}_3$ .

The crystallite size ( $d$ ), of the synthesized HAP powder calcined at 400 °C was calculated to be 8.7, 4.9 nm for planes (210) and (211). Moreover, the average crystallite size is 6.8 nm. In addition the average crystallite size of HAP supported 10 wt%  $\text{MoO}_3$  calcined at 400 °C is 11 nm.

### 3.3 Surface Area and Porosity

Adsorption–desorption isotherms of nitrogen gas were measured for the calcined products of AHM supported on nano hydroxyapatite at 400 °C in the air for 4 h and presented in Fig. 3. The specific surface area  $S_{\text{BET}}$  was obtained by applying the BET equation in its normal range of applicability (0.05–0.30  $p/p^0$ ) with cross-sectional area of  $\text{N}_2 = 16.2 \text{ \AA}$  and are represented in Table 1. Figure 3 shows that all isotherms of pure nHAP and loaded catalysts resulted in type II of Brunauer classification [34]. In addition, all catalysts exhibit a hysteresis loop, which closes at lower relative pressures. All hysteresis loops belong to types E with little of type A of de Boer's classification [35]. The results in Table 1 indicate that, the pure sample of HAP calcined at 400 °C exhibits  $S_{\text{BET}}$  value of

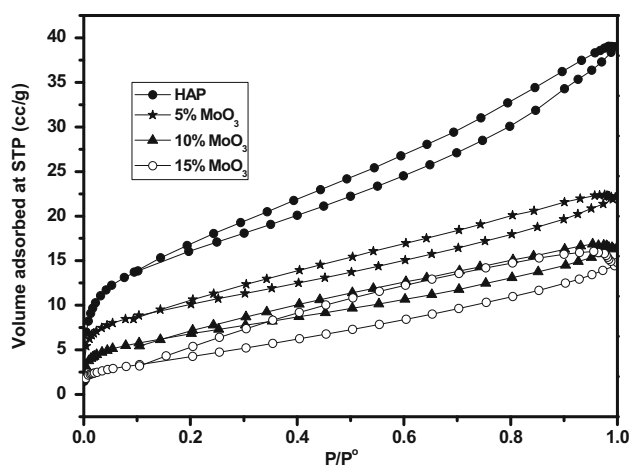


**Fig. 3** Nitrogen adsorption–desorption isotherms of pure HAP and  $\text{MoO}_3$  supported on HAP calcined at  $400\text{ }^\circ\text{C}$  for 4 h

$56.1\text{ m}^2\text{ g}^{-1}$ . The addition of AHM into HAP support led to a continuous decrease in  $S_{\text{BET}}$  values up to the addition of 15 wt%. This behavior may be attributed to the formation of  $\text{CaMoO}_4$  spinel which exhibits low surface area together with low surface area of pure  $\text{MoO}_3$ .

### 3.4 Assessment of Porosity of $\text{MoO}_3/\text{HAP}$ Catalysts

The assessment of porosity for pure HAP and supported  $\text{MoO}_3$  with (1–15 wt%) calcined at  $400\text{ }^\circ\text{C}$  was carried out by the application of the  $V_a - t$  plot method and the results are shown in Fig. 4. Also the  $S_t$  values were calculated from the slope of the straight lines of the investigated catalysts and are cited in Table 1. However, the shape of the  $V_a - t$  plots may indicate the type of existing porosity. Downward deviation indicates microporosity while upward deviation indicates the existence of wide pores, mesopores [36]. From Fig. 4 it can be seen that, the feature of the  $V_a - t$  plots of HAP and  $\text{MoO}_3$  supported on HAP catalyst exhibits a downward deviation up to the addition of 15 wt%, which is indicated microporous nature. These results demonstrate that the formation of new spinel does not change the micro porosity of HAP support.

**Table 1** Texture data of the  $\text{MoO}_3/\text{HAP}$  catalysts calcined at  $400\text{ }^\circ\text{C}$  for 4 h

Mixing %	$S_{\text{BET}}\text{ m}^2\text{ g}^{-1}$	$S_t\text{ m}^2\text{ g}^{-1}$	Total pore Volume ( $\text{cc g}^{-1}$ )	Average pore diameter (nm)
Pure HAP	56.1	55.2	0.0603	4.3
1 % $\text{MoO}_3$	47.3	47.0	0.0503	4.2
3 % $\text{MoO}_3$	40.6	40.2	0.0417	4.0
5 % $\text{MoO}_3$	35.4	34.3	0.0342	4.1
7 % $\text{MoO}_3$	29.0	28.1	0.0301	4.5
10 % $\text{MoO}_3$	22.2	22.2	0.0254	4.3
15 % $\text{MoO}_3$	8.8	8.8	0.0230	6.4

Figure 5 represents the pore volume distribution curves for pure HAP and supported with  $\text{MoO}_3$  calcined at  $400\text{ }^\circ\text{C}$ . Also, the total pore volume and average pore diameter were calculated from the desorption curves and presented in Table 1. It can be seen from this figure that the pore spectra of pure HAP calcined at  $400\text{ }^\circ\text{C}$  shows one sharp peak maximized at the value of  $r_p^-$  equal to 4.3 nm. This value again indicates that the HAP support exhibits microporous nature. Upon addition of  $\text{MoO}_3$  up to 10 wt%, the values of  $r_p^-$  are quite similar to that of pure HAP. On further increase the content of  $\text{MoO}_3$  up to 15 wt%, the mean pore radius increases to 6.4 nm. Moreover, the calculated particle sizes ( $D_{\text{BET}}$ ) of HAP and HAP supported with 10 wt%  $\text{MoO}_3$  calcined at  $400\text{ }^\circ\text{C}$  were found equal to 10 and 12 nm, respectively. These results are in a good agreement with that obtained from XRD calculations.

### 3.5 Acidity Determination

The catalytic dehydration of IPA over 10 wt%  $\text{MoO}_3$  supported on HAP calcined at  $400\text{ }^\circ\text{C}$  for 4 h was carried out and the results are shown in Fig. 6. The results revealed that the reaction products of IPA was propene (major) with acetone (minor) not exceed 5 %. However, the reaction of IPA does not provide information to distinguish between Lewis and Brønsted acid sites. So, the adsorption of PY and DMPY as a basic probes are better suited to differentiate between Lewis and Brønsted acid sites [37]. Consequently, the poisoning of the active surface sites of the catalyst in IPA conversion was performed by saturation of acid sites with injection of different volumes of PY or DMPY in the stream of the IPA reactant and the results are presented in Fig. 6. The results show that the injection of PY or DMPY led to a continuous decrease in the conversion of the IPA and the yield of propene up to the addition of  $1\text{ }\mu\text{l}$  then a steady state is reached. This behavior reflects that PY and DMPY decrease the conversion and yield of propene by 55 and 50 %, respectively. It is clear from this result that there is a little difference ( $\approx 5\%$ ) between the amounts adsorbed from PY and DMPY which is corresponding to the presence of Lewis acid sites. In addition

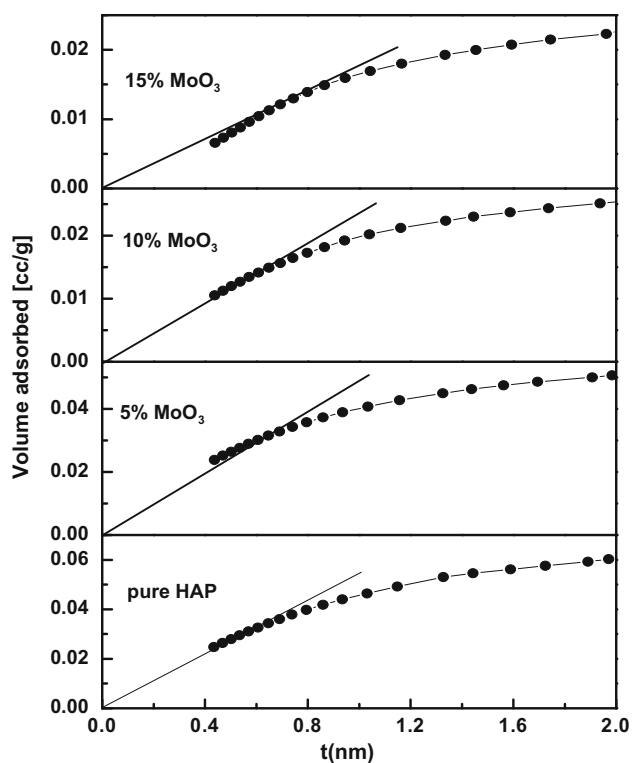


**Fig. 4**  $V_a - t$  plots of pure HAP and  $\text{MoO}_3$  supported on HAP catalysts calcined at  $400^\circ\text{C}$  for 4 h

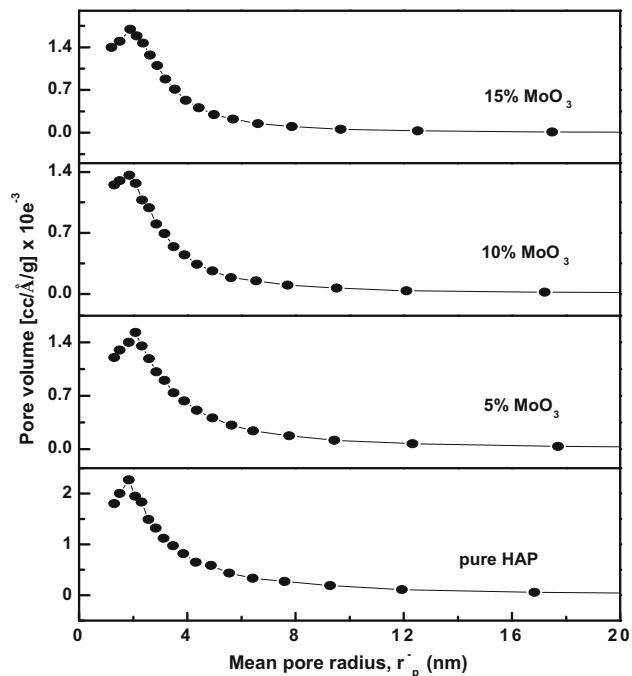


**Fig. 5** Pore volume distribution of pure HAP and  $\text{MoO}_3$  supported on HAP catalysts calcined at  $400^\circ\text{C}$  for 4 h

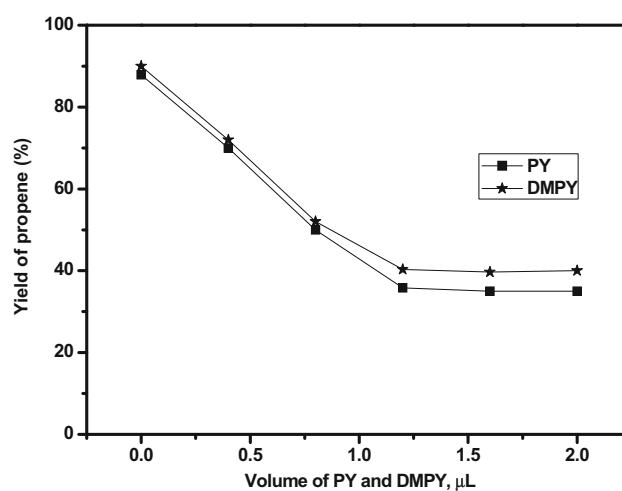


**Fig. 6** Activity variation of IPA with the volume of PY and DMPY over 10 wt%  $\text{MoO}_3/\text{HAP}$  calcined at  $400^\circ\text{C}$  in a static air atmosphere for 4 h

**Table 2** Activity variation of IPA over unsaturated and saturated 10 wt%  $\text{MoO}_3/\text{HAP}$  with PY and DMPY at different reaction temperatures

Reaction temp. ( $^\circ\text{C}$ )	% yield of propene		
	Unsaturated catalyst	Saturated catalyst with	
		PY	DMPY
125	0	0	0
150	25	10	15
175	51	24	29
200	75	52	57
225	95	85	90
250	95	95	95

$\approx 40\%$  of available acid sites still working to converting IPA to propene which confirms that, the PY or DMPY adsorbed on the catalyst surface did not poisoning weak acid sites. Therefore, from the above results we see that the distribution of the acid sites of the catalyst under investigation is ( $\approx 45\%$ ) Brønsted, ( $\approx 5\%$ ) Lewis and ( $\approx 40\%$ ) weak Lewis acid sites.

Moreover, the effect of reaction temperature on the dehydration of of IPA over 10 wt%  $\text{MoO}_3$  supported on HAP previously saturated with PY and DMPY was carried out and the obtained results are cited in Table 2. The results reveal that the adsorption of PY or DMPY retards the conversion activity of IPA more than that of unsaturated catalyst. In addition, the catalyst restored its activity (acidity) after removal of PY or DMPY on increasing the reaction temperature up to  $225^\circ\text{C}$ . The retardation of the

catalyst activity may be attributed to the bond strength between PY or DMPY and the acid sites. DSC curves of the desorption of PY from presaturated pure nHAP and 10 % MoO<sub>3</sub>/HAP catalysts are carried out and presented in Fig. 7. The DSC curve of pure HAP shows only an endothermic peak covered the temperature range from 40 to 103 °C. This peak may be attributed to the removal of physical adsorbed water and PY desorption from weak acid sites. On the other hand, the DSC curve of 10 % MoO<sub>3</sub>/HAP exhibits endothermic peak extended from 62 to 234 °C which minimized at 108 °C may be attributed to the desorption of PY from weak and moderate acid sites. In addition an exothermic peak extended from 235 to 355 °C and minimized at 290 °C corresponds to the presence of moderate acid sites. So, the above results reflect that, the available acid sites exhibit weak and moderate strengths.

### 3.6 Catalytic Activity

The catalytic dehydrogenation of methyl alcohol over different percentages loading of MoO<sub>3</sub> supported on HAP catalysts precalcined at 400 °C for 4 h was carried out at the reaction temperature of 400 °C. The analysis of the gas mixture after reaction revealed that formaldehyde formation was the major and formic acid was a minor product, and the experimental results are presented in Fig. 8. It

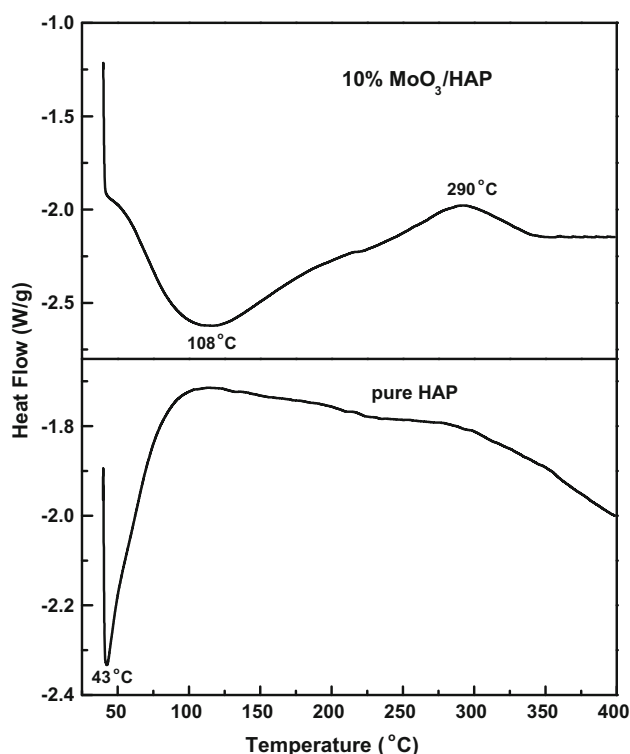


**Fig. 7** DSC curves of PY desorption from pure nHAP and 10 wt% MoO<sub>3</sub>/HAP presaturated catalysts

gives the relationship between the % conversion and yield with % mixing of MoO<sub>3</sub>. From this figure, one can observe that pure HAP precalcined at 400 °C exhibits some activity towards the formaldehyde formation ( $\approx 8$  %) and formic acid ( $\approx 17$  %). The addition of a little amount of MoO<sub>3</sub> (1 wt%) into HAP precalcined at 400 °C shows an observable increase in both methanol conversion ( $\approx 73$  %) and yield of formaldehyde ( $\approx 70$  %) while a sharp decrease in the yield of formic acid ( $\approx 3$  %). In addition, upon increasing % loading of MoO<sub>3</sub> up to 5 wt% a maximum yield of formaldehyde ( $\approx 97$  %) is obtained followed by a steady state up to the addition of 15 wt%.

The above results demonstrate that the % loading of MoO<sub>3</sub> to HAP is playing a main role in the activity and yield of formaldehyde. On the other hand, the catalyst containing 5 wt% MoO<sub>3</sub> precalcined at 400 °C exhibits excellent activity and selectivity towards the formation of formaldehyde. These results are very interesting not only for the high selectivity of the catalyst towards the formation of formaldehyde, but also in the capacity of the catalyst towards formaldehyde formation which is stable for a long duration time 90 h (not included).

On the other hand, formaldehyde is obtained from oxidative dehydrogenation of methanol by two processes, (i) on iron–molybdate catalysts and (ii) on silver based catalysts. In both processes, a conversion of about 99 and 92 % selectivity are obtained. The temperature of the reaction is 400 °C in the first and about 650 °C in the second process. In addition, iron–molybdate based catalysts get deactivation through a loss of molybdenum in a form of volatile compound and the presence of excess methanol also led to decrease in the activity [38]. Moreover, the silver process has high operating costs. Consequently, the comparison between our present work with the

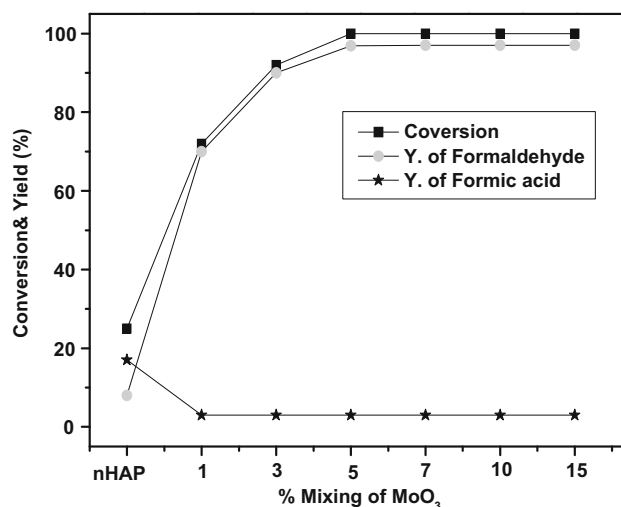


**Fig. 8** Catalytic oxidation of methanol over MoO<sub>3</sub>/HAP calcined at 400 °C for 4 h

two commercial processes of methanol oxidation to formaldehyde, it is remarkable that the yield of formaldehyde is 97 % over 5 wt% MoO<sub>3</sub>/HAP catalyst. So, our results demonstrate at least two advantages. Firstly, the high yield of formaldehyde is obtained. Secondly, the activity of the catalyst is stable for a long duration time (90 h).

However, methanol oxidation is a reaction well adapted to characterize the redox and acidic active species on the catalyst surface. The structural information at the molecular level about the catalytic sites can be deduced from the catalytic behavior of this reaction [1]. A selective formation of methylal ((CH<sub>3</sub>O)<sub>2</sub>CH<sub>2</sub>) can be assigned to a dual site, including a redox dehydrogenating site and a Lewis acid center, whereas the formaldehyde (CH<sub>2</sub>O) formation requires only a redox dehydrogenating site. Methyl formate (HCOOCH<sub>3</sub>) can be generated via an oxidation reaction (redox centers) followed by the dehydration (on acidic sites). The surface basic sites are responsible for the CO + CO<sub>2</sub> formation. The selective formation of dimethyl ether (CH<sub>3</sub>OCH<sub>3</sub>) is assigned to the presence of strong acid sites. In principle the Brønsted acidity [39, 40] is characteristic of oxides in which the transition element is in a high oxidation state, e.g. V<sub>2</sub>O<sub>5</sub>, MoO<sub>3</sub>, CrO<sub>3</sub>, etc. According to Davydov [39], the Brønsted acidity is responsible for the selective oxidation of methanol to formaldehyde. Klisurski et al. [41] results are in agreement with the above suggestions. The results of acidity determination Fig. 6, indicate the creation of Brønsted acid sites with intermediate strength existed on the catalyst surfaces as predicted from Fig. 7 exhibit a higher activity in methanol oxidation to formaldehyde [42]. This is probably due to the fact that impregnation ensures better dispersion of molybdenum trioxide in the HAP support. So, Mo cation selectivity interacts with hydroxyl groups basic nature and suitable strength leading to the formation of monolayer patches of MoO<sub>3</sub> support surface. Moreover, catalyst containing dispersed Mo centers on oxide supports are known to have high acid properties due to the development of molybdate and poly molybdate species possessing Brønsted and Lewis acid sites [43, 44]. The HAP surface contains hydroxyl groups which are weakly acidic, then the deposition of M–O phase is expected to give rise to a remarkable increase in acidity. Moreover, in the investigated catalyst containing 10 wt% MoO<sub>3</sub>, the FTIR spectra, Fig. 9 shows that a band of Mo–O stretching vibration in MoO<sub>4</sub><sup>2-</sup> tetrahedrons [45] at 774–905 cm<sup>-1</sup>. This result is in agreement with that reported by Crosman et al. [46] and Wakman et al. [47]. Furthermore, the formation of CaMoO<sub>4</sub> upon calcination of MoO<sub>3</sub> supported on HAP with different ratios at 400 °C is accompanying with Mo<sup>6+</sup>. So, the creation of Mo<sup>6+</sup> as Lewis with Brønsted acid sites may be active and play a main role for methanol oxidation to formaldehyde.

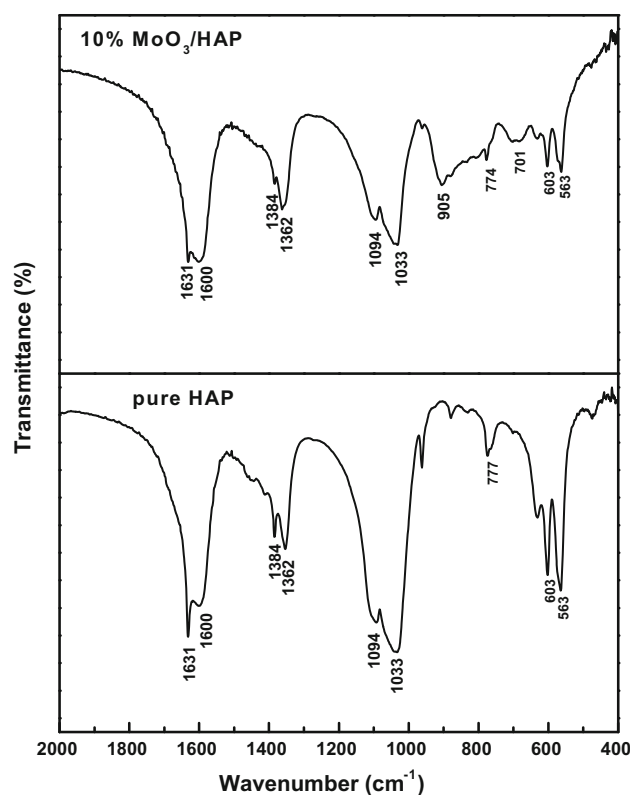


**Fig. 9** FTIR spectra of pure HAP and 10 % MoO<sub>3</sub>/HAP catalysts calcined at 400 °C

### 3.7 Conclusions

- HAP was synthesized via sol gel method and loaded with different ratios of MoO<sub>3</sub>.
- The catalysts calcined at 400 °C revealed that the formation of CaMoO<sub>4</sub> phase, which is confirmed by XRD and supported by DTA analysis.
- A continuous decrease in S<sub>BET</sub> values for all catalysts upon increasing the % loading of MoO<sub>3</sub>. The assessment of the catalysts porosity by V<sub>a</sub> – t plots and mean pore radius showed a microporous structure of all catalysts under investigation.
- The acidity determination confirmed that the major Brønsted and Lewis acid sites existed on the catalyst surfaces with intermediate strength were responsible for the higher activity towards formaldehyde formation.
- The maximum yield of formaldehyde (97 %) was achieved on the catalyst containing 5 wt% MoO<sub>3</sub>.

### References

1. Tatibouet JM (1997) J Appl Catal A 148:213
2. Stiles B, Koch TA (1995) Catalyst manufacture, vol 2. Marcel Dekker, New York, p 197

3. ECN (1994) Process Review, April 30
4. Chauvel R, Curty PR, Maux R, Petipas C (1973) *Hydrocarb Process* 52:179
5. Yang TJ, Lunsford JH (1987) *J Catal* 103:55
6. Matsuoka Y, Niwa M, Murakami Y (1990) *J Phys Chem* 94:1477
7. Kim DS, Wachs IE, Segawa K (1994) *J Catal* 149:268
8. Hu H, Wachs IE (1995) *J Phys Chem* 99:10911
9. Niwa M, Igarashi J (1999) *Catal Today* 52:71
10. Muragan R, Ramakrishna S (2005) *Comput Sci Technol* 65:2385
11. Kebby LC, Hall KW (1973) *J Catal* 29:144
12. Yasukawa A, Yokoyama T, Kandori K, Iswkawa T (2004) *Colloids Surf A* 238:133
13. Boucetta C, Casimi M, Ensuque A, Piquemal J-Y, Bozon-Verduraz F, Ziyad M (2009) *Appl Catal A* 356:201
14. Sugiyama S, Osaka T, Hirata Y, Sotowa K (2005) *Appl Catal A* 312:52
15. El-Kabouss K, Kasimi M, Ziyad M, Amar S, Bozon-Verduraz F (2006) *J Mater Chem* 16:2453
16. Pivtedu LD, Girona MI, Schlapbach L, Barbour P, Pilot JB, Gasser B (1999) *J Mater Sci Mater Med* 10:161
17. Gross KA, Chai CS, Kanangra GSK, Bin-Nissa B, Hanley L (1998) *J Mater Sci Mater Med* 9:839
18. Hwang K, Lim Y (1999) *Surf Coat Technol* 115:172
19. Haddow DB, James PF, Van-Noort R (1998) *J Sol-Gel Sci Technol* 13:261
20. Young RA, Holcomb DW (1982) *Calif Tissue Int* 34:17
21. Slosarezyk A, Stobierska E, Paszkiewicz Z, Gawlick M (1996) *J Am Ceram Soc* 79:2539
22. Yoshimura M, Suda H, Okamoto K, Ioku K (1994) *J Mater Sci* 29:3399
23. Said AA, Abd-El-Wahab MM, Alian AM (2014) *IOP Conf Mater Sci Eng* 64:012058
24. Bigi A, Boanini E, Rubini K (2004) *J Solid State Chem* 177:3092
25. Cullity BD (1967) *Elements of X-ray diffraction*, 3rd edn. Addison-Wesley, Reading
26. Said AA, Abd El-Wahab MM, Abd El-Aal M (2014) *J Mol Catal A* 394:40
27. Waterhouse GIN, Bowmaker GA, Metson JB (2004) *Appl Catal A* 265:85
28. Ramanan SR, Venkatesh R (2004) *Mater Lett* 58:3320
29. Han Y, Wang X, Li S, Ma X (2009) *J Sol-Gel Sci Technol* 49:125
30. Klinkaewnarong J, Swatsitang E, Maensiri S (2009) *Solid State Sci* 11:1023
31. Ryu J, Yoon J, Lim C, Oh W, Shim K (2005) *J Alloys Compd* 390:245
32. Yoon JW, Ryu JH, Shim KB (2006) *Mater Sci Eng B* 127:154
33. Eslami H, Solati-Hashjin M, Tahriri M, Bakhshi F (2010) *Mater Sci Poland* 28:5
34. Brunauer SJ, Deming LS, Deming W, Teller E (1940) *J Am Chem Soc* 62:1723
35. de Boer JH, Everett EP, Stone FS (eds). (1958) *The structure and properties of porous materials*. Butterworths, London, p 68
36. El-Nabarawy TH, Fagal GA, El-Shobaky GA (1989) *Bull NRC Egypt* 14:1
37. Said AA, Abd El-Wahab MMM, Alian AM (2007) *J Chem Technol Biotechnol* 82:513
38. Soares APV, Portela MF, Kiennemann A, Hilaire L, Millet JMM (2001) *Appl Catal A* 206:221
39. Davydov AA (1990) *Infrared spectroscopy of adsorbed species the surface of transition metal oxides*. Wiley, Chichester
40. Hadjiivanov K, Busca G (1994) *Langmuir* 10:4534
41. Klissurski D, Petridis D, Abadzhieva N, Hadjiivanov K (1996) *Appl Clay Sci* 10:451
42. El-Awad AM, Hassan EA, Said AA, AbdEl-Salaam KM (1989) *Monatshfte fur Chemie* 120:199
43. Damyanova S, Grange P, Delmon B (1997) *J Catal* 168:421
44. Massoth PE (1978) *Adv Catal* 27:265
45. Crosman A, Gelbard G, Poncelel G, Parvulescu VI (2004) *Appl Catal A* 264:23
46. Wakamura M, Kandori K, Iskikawa T (1998) *Colloids Surf A* 142:107
47. Kato A, Shi SO, Shishido T, Yamazaki M, Iida S (2005) *J Phys Chem Solids* 66:2079